

# Wake instabilities and flow state analysis of the flow past a prolate spheroid

R. He<sup>\*</sup>, Zhiguo Zhang<sup>\*</sup> and Xianzhou Wang<sup>\*</sup>  
Corresponding author: zzg@hust.edu.cn

\* School of Naval Architecture & Ocean Engineering, Huazhong University of Science and Technology, Wuhan, 430074, CHINA

**Abstract:** The viscous flow past a prolate spheroid, which is always complicated and often three-dimensional, has fascinated scientists in fluid mechanics and aerodynamics for decades. The objective of this paper is to investigate the wake instabilities and flow state of the flow past a 6:1 prolate spheroid at 45° angle of attack by means of Large-Eddy simulations (LESs). The calculation was performed at a Reynolds number of 10000, based on the free stream velocity  $U_0$  and minor axis length  $D$ . The helical vortex tube is formed by the vortex sheets generated by the three-dimensional separating flow on the side of prolate spheroid. The fluid generated vorticity after separating from the prolate spheroid along the inclined line of separation. The vorticity component along the line of separation results in the rolling of vortex sheets while the one perpendicular to separation line contributes to the axial velocity. These two components form the helical vortex tube together. The right tube develops along major axis of spheroid from the very beginning and then skews rightward because of asymmetry of the whole flow field. The complex vortex composition is observed and helical advance changes during the formation of helical vortex tube. The helical vortex is dextral with jet-like axial velocity profile in front of a specific position while it suddenly becomes sinistral with wake-like axial velocity profile behind the position, which is the feature of vortex breakdown.

*Keywords:* Wake instability, Computational Fluid Dynamics, LES, Aeroacoustics.

## 1 Introduction

The flow around submarines as well as other underwater vehicles are usually complicated and three-dimensional (3D). Motions of these objects are examples of a significant role of prolate spheroid, which can be considered as a simplified model. The flow past a prolate spheroid by means of Direct Numerical Simulation (DNS) and Large-Eddy Simulations (LES) at different angle of attack have been studied<sup>[1-5]</sup>. The prolate spheroid is geometrically simple but the flow is complex, characterized by cross-flow separation, wake asymmetry and transition. Apart from the complexity of flows, undesired phenomena, such as loss of lift, increase of drag and unsteady forces and moments, occur when the angle of attack presents. The great importance of prolate spheroid in engineering have fascinated scientists in fluid dynamics and aerodynamics for decades. Besides, researches on prolate spheroid vary with different combinations of parameters, such as the ratio between the semi-major and semi-minor axes, angle of attack and Reynolds number. The change of each parameters has an influence on the flow and therefore people need more effort to gain a comprehensive insight on

prolate spheroid.

The main purpose of this paper is to investigate the instability of asymmetric wake behind a 6:1 inclined prolate spheroid by means of Large-Eddy simulations (LESs). The asymmetric wake arises due to flow instabilities which develop above a certain Reynolds number. Since the frequency analysis can illustrate lots of features of instability, this paper mainly focus on frequency domain.

Firstly, we obtained turbulence energy spectra concerning Strouhal number at 25 points by means of simple FFT. In this way, we can get more information than the Fourier transform of the velocity amplitude. These energy spectra were used when we determined the flow state at  $Re=10000$ . Then the Fourier transform of the force was conducted in order to obtain two dominant frequency. In present study, two dominant frequency,  $St_1=0.1462$  and  $St_2=0.2436$  could be observed. Generally, there are two types of the instability feature captured on the frequency domain, i.e. the shear layer instability and the vortex shedding frequency. The former type usually shows high frequency characteristic, with the curve on frequency domain behaving flat and smooth and spanning a slightly larger range. While another one shows in low frequency region, observed as a peak, such as von Karman Vortex Street behind a two-dimensional cylinder where Strouhal number  $\approx 0.21$  at  $Re = 300 \sim 3 \times 10^5$ . However, when we considered  $St_2=0.2436$  as a secondary harmonic frequency, the low frequency,  $St_1=0.1462$ , was attributed to three-dimensional effect.

The reason to study the flow state is that the instability problem always have a relationship with the transition. To be specific, it is because of the instability, the steady laminar flow develops into the turbulence. Hence the Kolmogorov's hypothesis was used to judge the flow state. However, due to the processing method and numerical errors of LES, some part of the figure got distorted.

The organization of this paper is as follows. Section 2 is devoted to describe LES and sub-grid scale model used in this work is present. This is followed in section 3 by the description of flow configuration and grid independence study. In section 4, numerical analysis and discussion are given. Finally some conclusions are drawn in Section 5.

## 2 Numerical method

### 2.1 Large-Eddy Simulation

As numerical methods are developed to compute the flows encountered in many areas, one major problem that remains to be solved is how to take turbulence effects into account. Turbulent flows are composed of a set of movements on very various scales, especially when the characteristic Reynolds number of the flow is much greater than unity. The ratio of the largest to the smallest length scales can be extremely high. It is generally agreed that the Navier-Stokes equations are valid for describing such flows, but the direct numerical solution of these equations is difficult in practice due to the large number of degrees of freedom to be taken into account to correctly represent the flow. One technique to consider turbulence effects is Large-Eddy Simulation (LES), which divides the eddy in turbulence into the large scale and the small scale [6].

LES, firstly proposed in 1963, is a mathematical model for turbulence in computational fluid dynamics. The simulation of turbulent flows by numerically solving the Navier-Stokes equations requires resolving a very wide range of time and length scales, all of which affect the flow field. LES is fast becoming a viable alternative to solve this problem.

In LES, the large eddy have strong interaction with the mean flow, and a strong dependent relationship exists in its initial condition and boundary geology; the state and the intensity of large eddy vary as the flow, which is highly anisotropic. Most of the transportation of mass, momentum, and energy depend on the large eddy. However, the small eddy have less relationship with the mean flow and the boundary condition, and therefore can be regarded as isotropic, which is more independent of the specific flow. In LES only the contribution of the large, energy-carrying structures to momentum and energy transfer is computed exactly, and the effect of the small scales of turbulence

is modelled. As the small scales are the most computationally expensive to resolve, LES is able to reduce the computational cost greatly compared to DNS, in which all the turbulent motions are resolved accurately. In addition, since the small scales tend to be more homogeneous and less affected by the boundary conditions than the large ones, it might be possible that their models can be simpler and require fewer adjustments when applied to different flows than similar models for the Reynolds-averaged Navier–Stokes (RANS) equations.

LES are based on the use of a filtering operation: a filtered variable, denoted by an overbar, is defined as[7]

$$\bar{f}(x) = \int_D f(x')G(x, x', \Delta)dx' \quad (2.1)$$

where D is the entire domain, G is the filter function and the filter width is denoted here by  $\Delta$ . If the filtering operation (2.1) is applied to the governing equations, one obtains the filtered equations of motion. For an incompressible flow of a Newtonian fluid, they take the form:

$$\frac{\partial \bar{u}_i}{\partial x_i} = 0 \quad (2.2)$$

$$\frac{\partial \bar{u}_i}{\partial t} + \frac{\partial}{\partial x_j} (\bar{u}_i \bar{u}_j) = -\frac{1}{\rho} \frac{\partial \bar{p}}{\partial x_i} - \frac{\partial \tau_{ij}}{\partial x_j} + \nu \nabla^2 \bar{u}_i \quad (2.3)$$

where  $\bar{u}_i$ ,  $i = 1, 2, 3$  is the filtered velocity component in streamwise (x), crossflow (y) and spanwise (z) direction respectively ( $x_i$  is assigned to the respective directions),  $\rho$  is the density of the fluid and p is the filtered pressure. All these filtered quantities are paramount and they must be measured physically and accurately if we want to apply LES to solving practical flow problems [8].

These equations govern the evolution of the large, energy-carrying scales of motion. While the effect of the small scales is described through a residual stress term, namely the subgrid-scale (SGS, a more appropriate definition is subfilter-scale, i.e. SFS) stress,  $\tau_{ij} = \bar{u}_i \bar{u}_j - \overline{u_i u_j}$ , in order to use a SGS model and get a full solution for filtered equations.

LES is used not only on academic researches but also in engineering, such as airfoil [9], a plane impinging jet [10], turbine and submarine [11]. As the present study mainly focus on the flow field at  $ReD=10000$ , the reliability and capability of LES at high Re number is particularly significant. In 2000, G. Q. Chen et al pointed out that LES hold great promise at the high Re number of practical engineering interest with the development of LES models that could make good use of the information on the energy cascade process from large scales to small ones, such as dynamic subgrid-scale model [12]. Recently, A. Feymark et al [12] have investigated four cases in their study, to improve the understanding of high Re number turbulent flows around realistic objects and to examine the capability of LES for such flow configurations. After a short review of LES and subgrid models, focusing on subgrid viscosity and mixed models, near-wall models and numerical methods, four experimentally examined flows, containing different surface flow and separation physics, are computed, validated and analyzed. Although there are some differences, the results match well with experiment data, which indicates LES is a reliable method.

In the past decades, LES have developed fast and researchers have made advances in this method. For example, efficient treatment of complex geometries for LES was put forward [14], and two numerical methods (immersed boundary method and an unstructured mesh scheme [15]) and a parallel, finite-volume algorithm [16] have been developed. These advances enable the application of LES in complex domains. However, there are also challenges that pervade the transition process from RANS to LES in industry. These challenges are attributed to several factors inherent to LES itself, including the choice of filtering, the problems posed by numerically solving the equations, validation of the computation results, closure of modelling and near-wall treatment [17].

## 2.2 Smogorinsky-Lilly Model

If the filtered small scale fluctuation can achieve local equilibrium, then the energy transform from the solved scale to the modeled scale is equal to the turbulence dissipation rate. The subgrid-scale motions are modelled by a commonly used Smagorinsky model, the most widely used SGS model. It assumes that the eddy viscosity is proportional to the subgrid scale characteristic length and to the characteristic subgrid scale velocity. This model could be summarized as

$$\tau_{ij} - \frac{1}{3} \tau_{kk} \delta_{ij} = -2\mu_t \bar{S}_{ij} \quad (2.4)$$

where  $\overline{S}_{ij}$  is strain rate tensor and  $\overline{S}_{ij} = \frac{1}{2} \left( \frac{\partial \overline{u}_i}{\partial x_j} + \frac{\partial \overline{u}_j}{\partial x_i} \right)$ , and  $\mu_t$  is subgrid-scale turbulent viscosity coefficient.

In the Smagorinsky-Lilly model, the eddy viscosity is modeled by  $\nu_t = \rho(C_s \Delta)^2 |\overline{S}|$ , where the filter width is usually taken to be  $\Delta = V^{1/3}$  ( $V$  is the volume of the computational cell) and  $\overline{S} = \sqrt{2\overline{S}_{ij}\overline{S}_{ij}}$ .  $C_s$  is the Smagorinsky constant, and is the local grid scale. The Smagorinsky constant is fixed;  $C_s = 0.1$  in the present study. Lilly derived a value of 0.23 for  $C_s$  for homogeneous isotropic turbulence in the inertial subrange. However, this value was found to cause excessive damping of large-scale fluctuations in the presence of mean shear and in transitional flows as near solid [18][19].

### 3 Flow Configuration and Grid Independence Study

#### 3.1 Flow Configuration

For the prolate spheroid used in this paper, the ratio between the semi-major and semi-minor axes, namely the aspect ratio, is 6:1. The equatorial diameter  $D$  of prolate spheroid in current cases is 0.02 m. The geometrical arrangement for the prolate spheroid in computation domain is shown in Figure 1. The geometrical configuration where the major axis of the prolate spheroid is fixed at a  $45^\circ$  angle of attack with respect to the uniform inflow  $U_0$ . The prolate spheroid is placed in a computational domain with an upstream length  $8D$ , a downstream length  $30D$ , the width  $21D$  and the height  $24D$ .

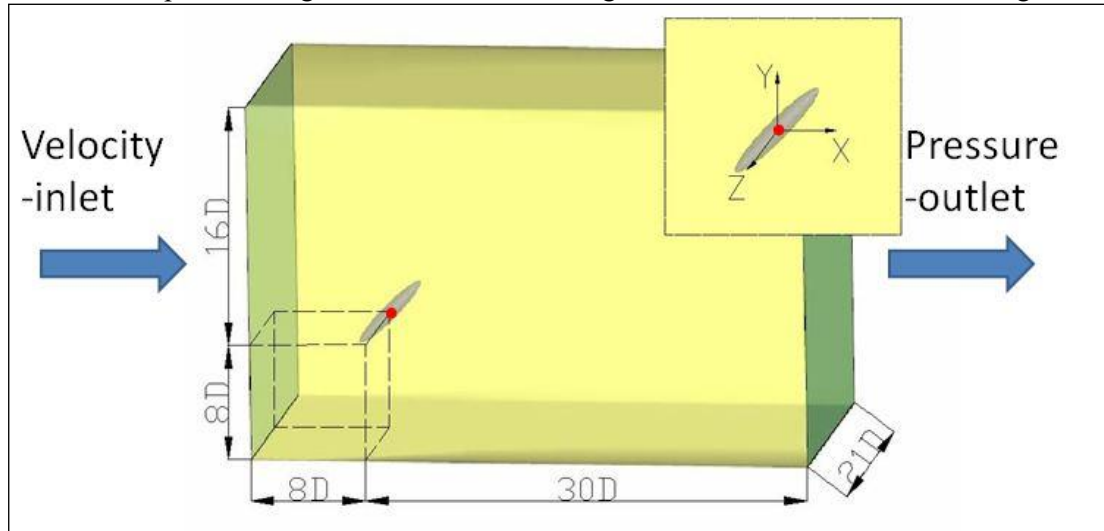


Figure 1 Flow configuration and orientation of the global coordinate

The Reynolds number  $ReD$  in this study is 10000, where  $ReD = U_0 D / \nu$  is based on the equatorial diameter  $D$ , the uniform inflow velocity  $U_0 (0.5, 0, 0)$  and the kinematic viscosity  $\nu$  of the fluid.

The topology of the computation domain is presented in Figure (a). A central block with scale of  $7.94D \times 3.08D \times 2.94D$ , shown in Figure (b), wraps the spheroid with finest mesh in order to ensure an accurate result of the body force. Near wall view of surface grid is also shown in Figure (c). The non-dimensional near wall distance ( $y^+$ ) for all the mesh are maintained to be less than 1. The blocks behind the spheroid gradually bending from  $45^\circ$  to  $0^\circ$  and wrapping the main vortex structure, the shape of which is obtained from pre-test, are also arranged with fine mesh to capture the characteristic of the wake field.

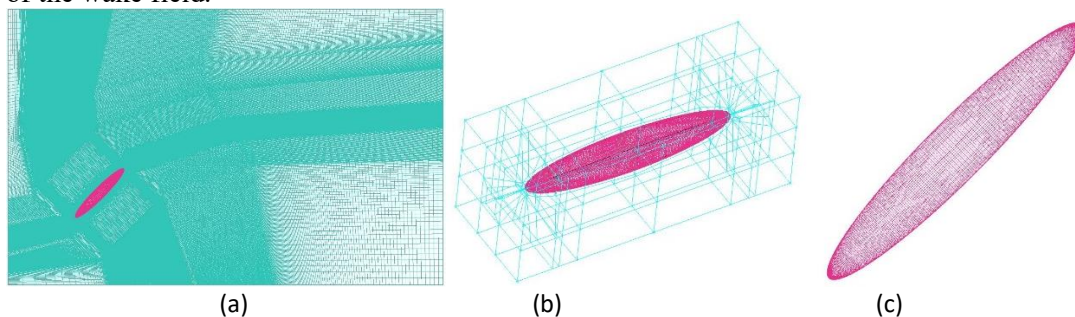


Figure 2 The topology of computational domain (b) The central block wrapping the prolate spheroid (c) Near wall view of surface grid

With regard to boundary conditions, at the inlet, a uniform flow with velocity  $U_0$  (0.5, 0, 0) is prescribed and at the outlet is defined as pressure-outlet (0 Pa). A non-slip boundary condition is imposed on the surface of the spheroid and the side of the domain is defined as symmetry.

As mentioned in Section 2, the Smagorinsky-Lilly model is employed with  $C_s=0.1$ . The solution method of pressure-velocity coupling is SIMPLEC. For the spatial discretization, the least square cell based method is performed for gradient, a second order method for pressure and bounded central differencing method for momentum. The bounded second order implicit method is used for transition formulation.

To facilitate the forthcoming discussions, the force coefficients here are defined with the same method with Jiang.F [4]:

$$C_{p_i} = \frac{F_i}{\frac{1}{2}\rho U_0^2 \frac{\pi}{4} d^2} \quad (3.1)$$

where  $F_i$  is the  $x_i$ -components of the force vector  $\vec{F}=(F_x, F_y, F_z)$  which the viscous fluid exerts on the spheroidal body. Here,  $d$  is the diameter of a volume-equivalent sphere which for the 6:1 prolate spheroid becomes  $d = 1.817D$ .

### 3.2 Grid Independence Study

The grid independence study is simply illustrated with the mean values of forces coefficients in  $x$  and  $y$  direction, which were defined above. The Table 1 presents the mean values of  $C_{fx}$  and  $C_{fy}$ .

Case	Coarse	Medium	Fine	Deviation	
Grid cells	21M	32M	50M	C&M	M&F
Time step	0.0002s	0.0002s	0.0002s		
$C_{fx}$	0.7127	0.7086	0.7120	0.58%	0.48%
$C_{fy}$	-0.768	-0.765	-0.772	0.39%	0.86%

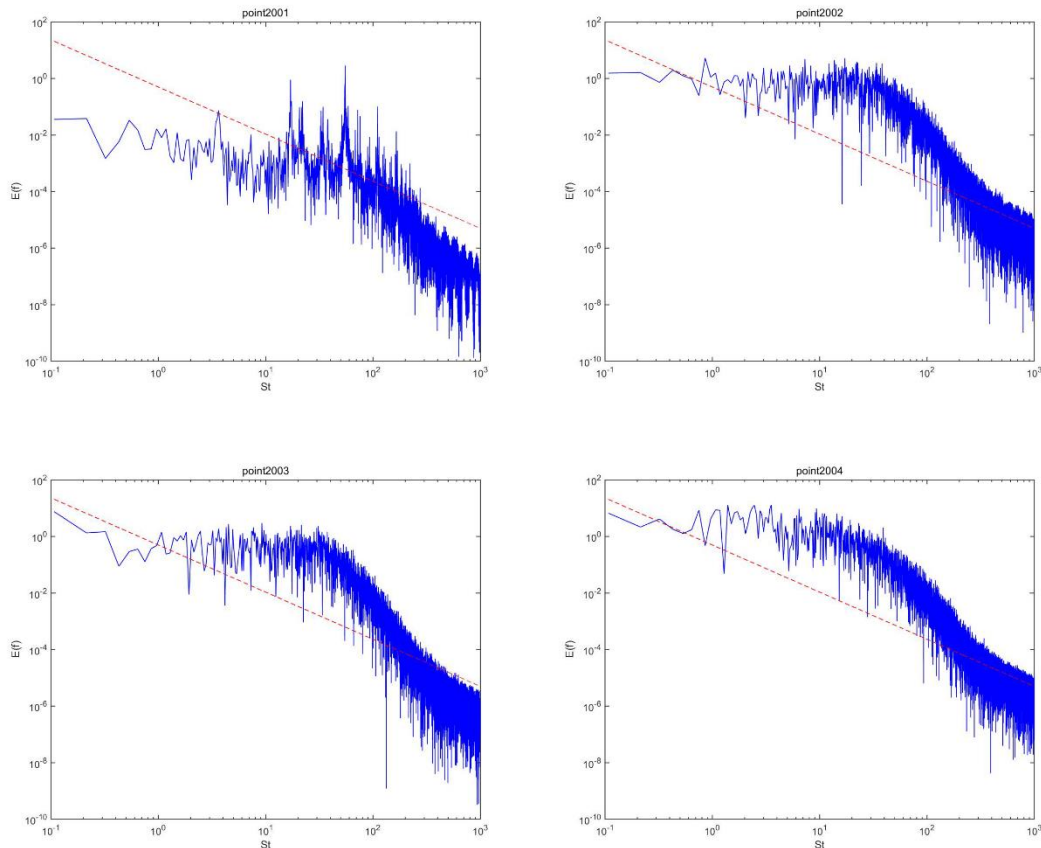
In this study, three different types of grid cells are employed. In the three grid configurations, the data obtained from the coarse mesh simulation are higher than those from the other meshes, except the value of  $C_{fy}$  obtained from fine mesh simulation. With the increase of the  $ReD$ , the  $C_{fx}$ , i.e. the  $C_{fd}$ , declined, which match well with the basic regulation between  $ReD$  and resistance in cases of other geometry. Also, from the table above, it is obvious that deviation between different cases is extremely low, with difference of all cases less than 1%. To be specific, the differences in  $C_{fx}$  and  $C_{fy}$  between medium and fine grids are 0.48% and 0.86% respectively. As these values in three cases are already indistinguishable, the comparisons support the adequacy of fine mesh at  $ReD = 10000$ . Therefore, fine grid mesh is used for the following simulation based on the available computational resources and the pursuit of high accuracy.

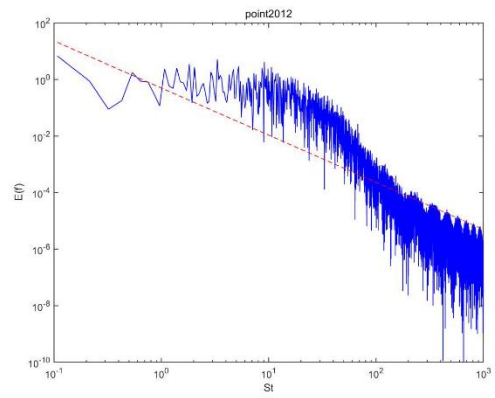
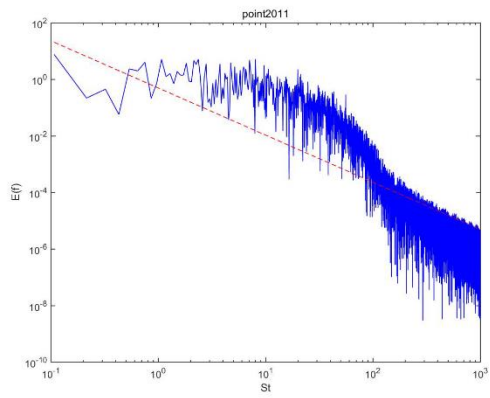
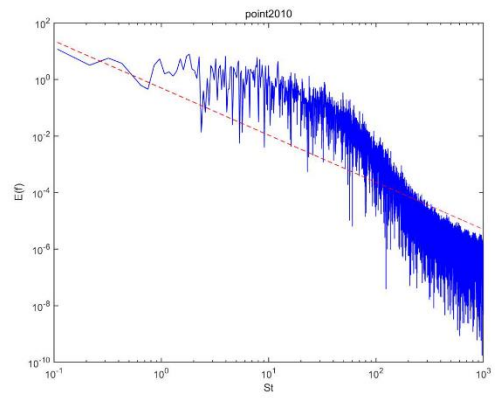
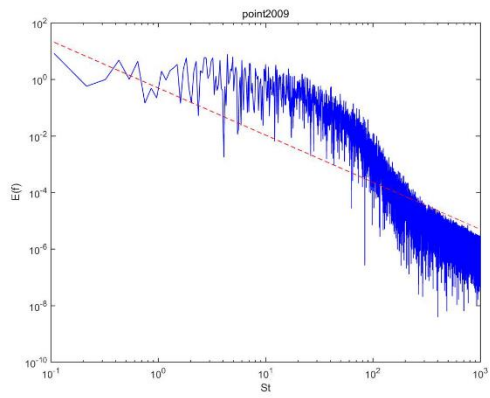
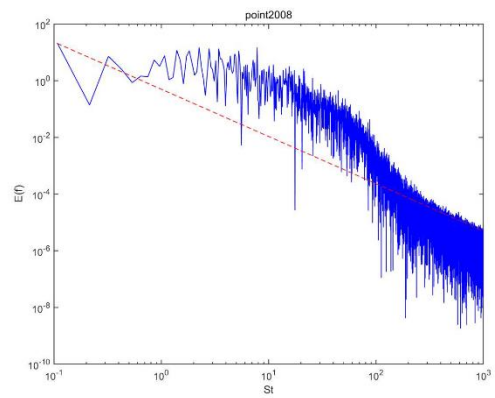
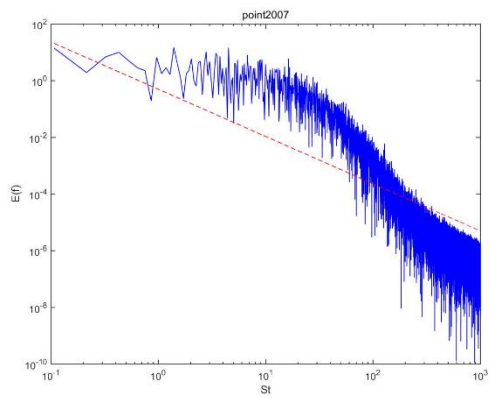
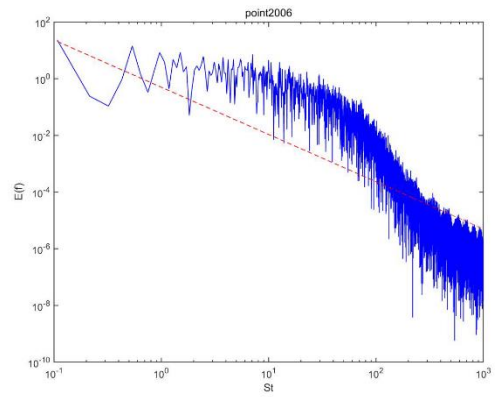
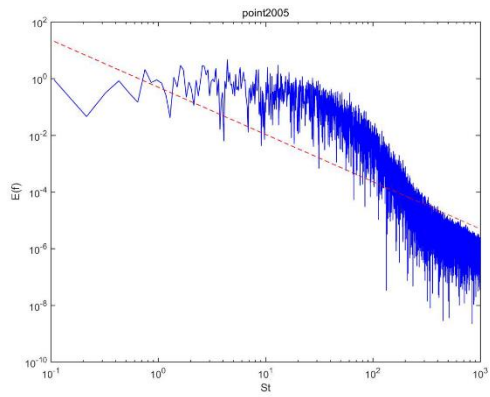
## 4 Numerical analysis and discussion

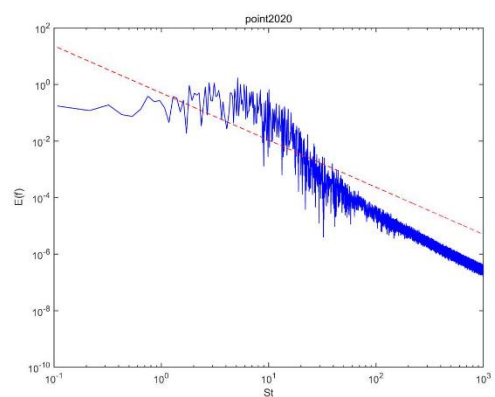
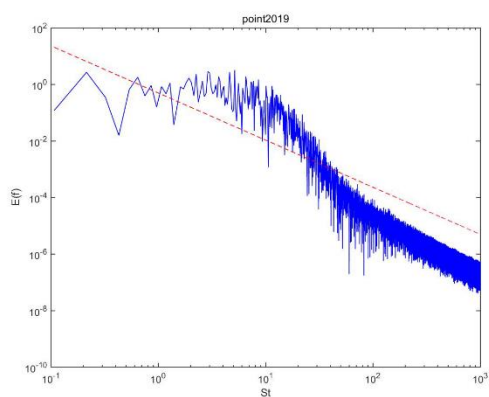
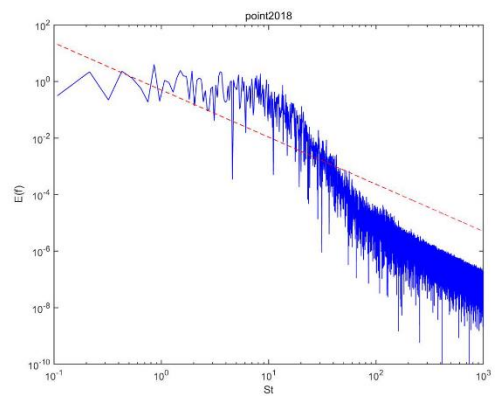
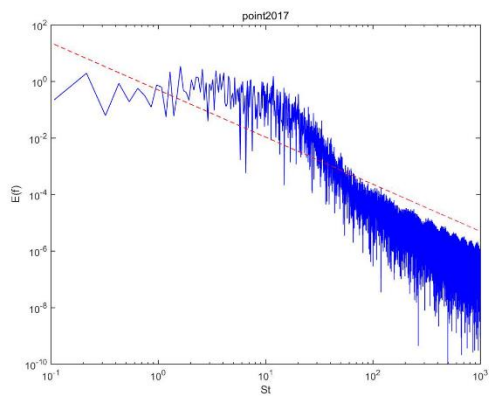
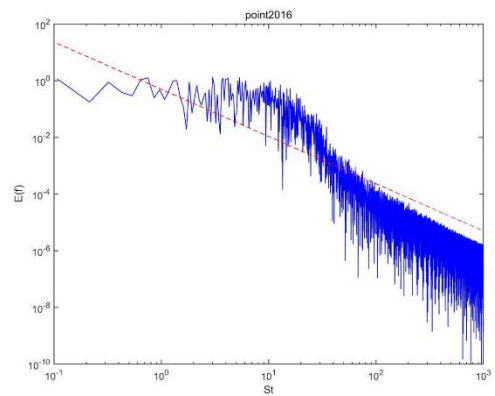
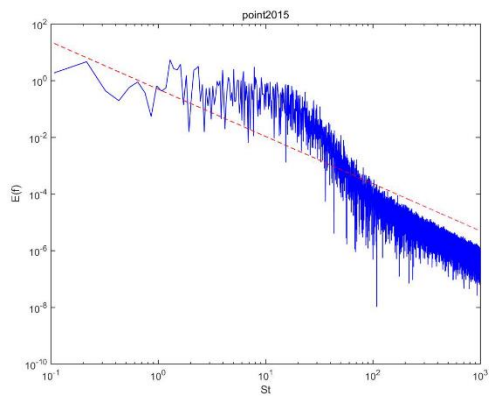
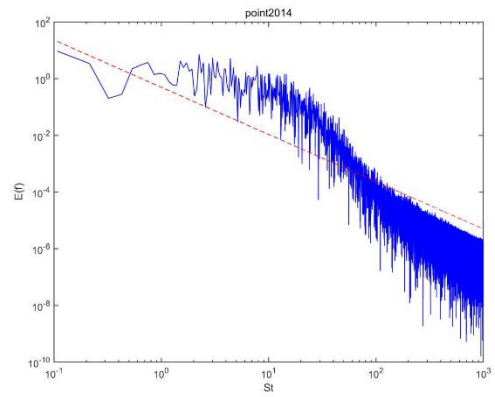
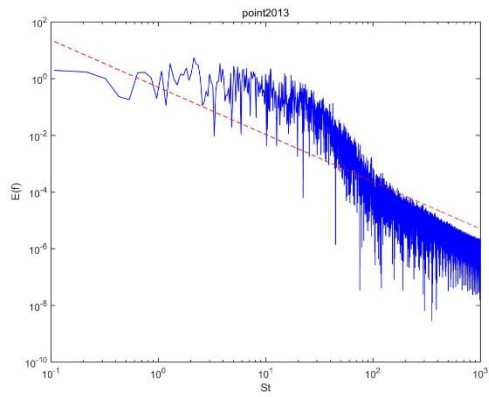
### 4.1 Wake instabilities and spectrum analysis

Asymmetric wakes, a conspicuous phenomenon in the flow fields of sharp-nose slender forebodies (e.g. a cone-cylinder), always arise at high attack angles because of flow instabilities. The origin of such instability has triggered debates for decades and there are two opposing standpoints: convective and global instability [20]. One of the principle pieces of evidence for the convective instability of the vortex wake is the necessity for an initial perturbation, such as a small bump or an actuator on the models. In the case of convective instability, all disturbances in a flow will be convected away once the initial source of the disturbances has been removed. It is assumed that small asymmetries of the models result in initial perturbation that is then amplified in the wake. On the contrary, if an initial disturbance is not required in an asymmetric wake, the global instability should be regarded as the accurate instability mechanics for the asymmetric wake. As in present study, no such disturbance was exerted in any location of the flow field, and all the boundary condition, the topological structure and the distribution of the grids is totally symmetric about  $z=0$  plane, it's therefore assumed that the global instability could explain asymmetric wake.

In Figure , 25 turbulence energy spectra of different points are present in order to have a comprehensive understanding of the frequency component of the whole flow field.







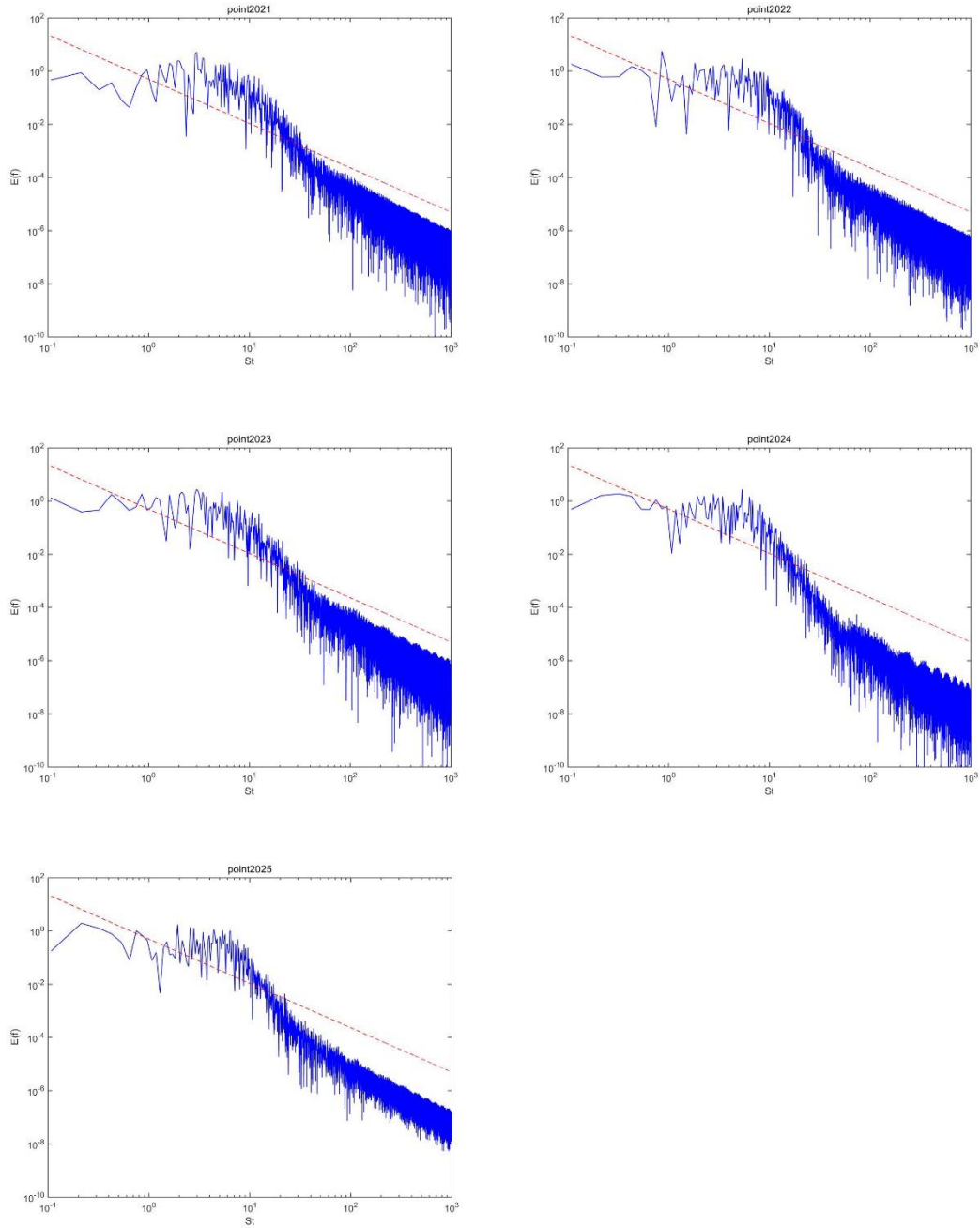


Figure 3 25 turbulence energy spectra of different monitor points and the red line indicates the Kolmogorov's  $-5/3$  reference line

Generally, the correct processing method is to add window functions to the original data before we do the FFT to obtain smooth curves, in order to minimize the effect of spectral leakages. Basically, what a window function does is that it tapers the finite length sequence at the ends, so that when tiled, it has a periodic structure without discontinuities, and hence less spectral leakage. However, these smooth curves with less noise signal require more data, and therefore more computational time and power, which can be hardly achieved in present study. Therefore, simple FFT is employed to obtain all the turbulence energy spectra. Nevertheless, even if the data in present study didn't get the average-treatment, the dominant frequency

obtained still should not be regarded as “coincidence” because the number of point we selected in the flow field is quite adequate, and they show the similar dominant frequency.

Table 2 The coordinate of monitor points

point	coordinate			point	coordinate			point	coordinate		
	x/D	y/D	z/D		x/D	y/D	z/D		x/D	y/D	z/D
2001	2	0.9	0	2010	12	4	0.5	2018	20	4	0.5
2002	4	2.2	0.5	2011	13	4	0	2019	21	4	0
2003	4	2.2	0	2012	14	4	-0.5	2020	22	4	-0.5
2004	6	3	-0.5	2013	15	4	0	2021	23	4	0
2005	6	3	0	2014	16	4	0.5	2022	24	4	0.5
2006	8	3.3	0.5	2015	17	4	0	2023	25	4	0
2007	8	3.3	0	2016	18	4	-0.5	2024	27	4	0
2008	10	3.9	-0.5	2017	19	4	0	2025	29	4	0
2009	11	4	0								

The locations of these point, as listed in Table 2 The coordinate of monitor points, are selected carefully according to some principles. These points start at  $x = 2D$  and end with  $x = 29D$  along  $x$ -axis so they can represent the whole flow field. For the  $z$  direction, they are arranged in three planes, i.e.  $z=0, 0.5,$  and  $-0.5$ , as asymmetry is one of the most important feature in this flow field. The selection of  $y$ -coordinate is based on the development of the vortex tube.

From turbulence energy spectra, it is hard to observed the dimensionless dominant frequency  $St=fD/U_0$ . One reason is the error caused by simple FFT. As mentioned before, the correct procedure is to use window functions, while it is not realizable in current study. Another one is that the amount of data is inadequate. The Fourier transform of force  $F = \sqrt{F_x^2 + F_y^2 + F_z^2}$  is given in Figure to give a better understanding of the effect of shortage of data. The data obtained by Fourier transform is marked by “×”. Obviously, the spacing of adjacent point along the horizontal axis is relatively large, which may bring error when we determine dimensionless dominant frequency in low-frequency area. In other words, the more data we get, the smaller spacing and the more accurate result can be obtained.

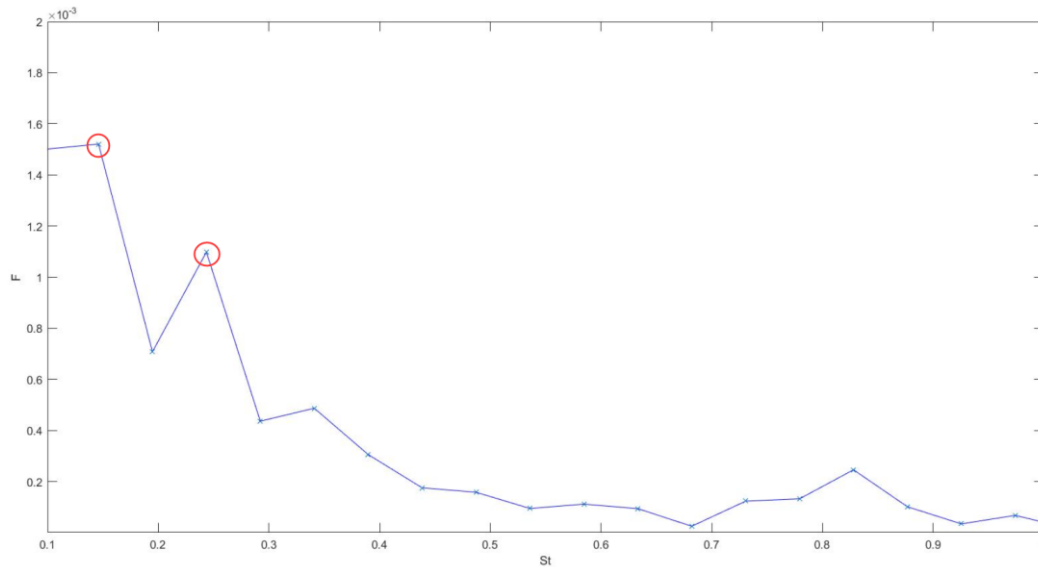


Figure 4 The Fourier transform of the force with two dominant frequency marked by red circle

While in Figure, two dominant frequency,  $St_1=0.1462$  and  $St_2=0.2436$  can still be observed. In Jiang. F's study [4], two dominant frequency is  $St_1=0.0733$  and  $St_2=0.15$ , see Figure . As  $St_2 \approx 2 St_1$ ,  $St_2$  should be regarded as a secondary harmonic frequency. Although a double relationship is captured in current study, the result is quite different with Jiang's. Therefore, the most important frequency is  $St_1=0.1462$ . In general, the low frequency is always related to vortex shedding. However, the dominating frequency  $St_1$  is lower than vortex shedding frequency, such as a typical von Karman vortex street behind a two-dimensional cylinder where  $St \approx 0.21$  and no such phenomenon is observed in this study. According to Jiang's study [4], this low frequency is the very-low-frequency three-dimensional effect, another type of instability that is less known. Such 3-D effect were first hypothesized by Ayoub and Karamcheti[21] as a possible cause of very-low-frequency unsteadiness. However, what is different with the results in present study is the almost in all cases where a very-low-frequency has been reported, there is not the dominant frequency. The alternative explanation has recently been put forward by Ma and Liu [22]. In their study, they observed a dimensionless frequency of 0.054 in the asymmetric wake behind an ogive-cylinder body at  $70^\circ$  angle of attack by means of LES. The very-low-frequency observed was associated with a vortex pair oscillating around the asymmetric mean flow. No such phenomenon could be detected in the present wake flow. However, while their wake was associated with a vortex pair oscillating around the mean flow, this phenomenon could not be detected in this study.

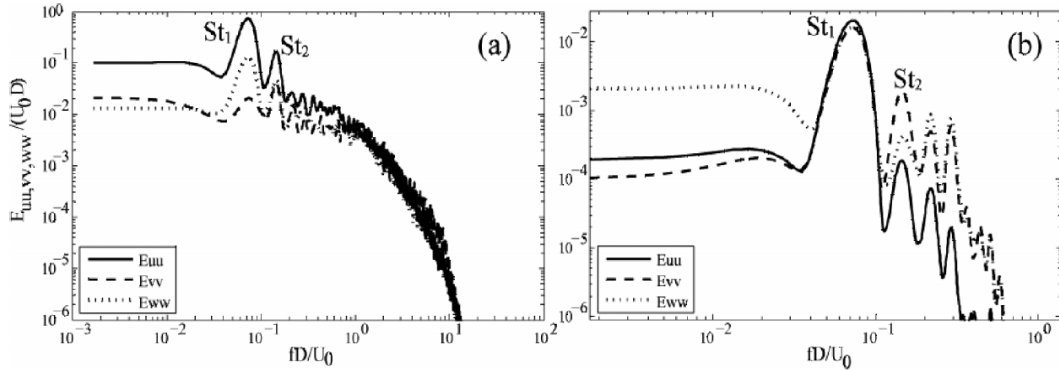


Figure 5 Energy spectra of the three velocity components in Jiang F's study. (a) In the intermediate wake at  $x/D=4$ ,  $y/D=2$ ,  $z/D=1$ ; (b) near the spheroid at  $x/D=0$ ,  $y/D=-1$ ,  $z/D=0.31$ .

#### 4.3 Flow state analysis and Kolmogorov's -5/3 law

The turbulence energy spectra obtained in this study show a steeper slope than the reference line, see Figure . Which means the amount of energy passed down from the large scales of motion to the smaller eddies is less than the amount defined from Kolomogorov's -5/3 law. Take the case in this study as an example, with the length of major axe of the prolate spheroid set as  $6D = 0.12\text{m}$ , and the velocity  $0.5\text{m/s}$ . We can get a time scale with  $T=0.24\text{s}$  and corresponding frequency at  $4.2\text{ Hz}$ , which means the largest eddy in this flow field (no larger than the object itself ) possess the  $4.2\text{ Hz}$  frequency. In this way, the range deserves our attention should be  $f=1\sim 10\text{ Hz}$ , which section is used to compare with the reference line.

These energy spectra give a simple and clear conclusion that the Reynolds number in present study is not high sufficiently to achieve the turbulence state. On the other hand, energy spectra at some points, such as point2008 and 2010, match well with the reference line in the range of  $f=1\sim 10$  Hz. In Jiang's study [4], the slope is steeper than that in present study, and the conclusion was drawn that the flow field at  $ReD = 3000$  was in transition state, taking the degree of the chaotic of the flow and steeper slope than the reference line into consideration. This conclusion is reasonable based on DNS method, in Figure 6 The difference in LES and DNS in the energy spectrum in terms of Kolomogorov's  $-5/3$  law, yet the error that LES itself brings should not be ignored. In other words, the energy dissipation (i.e. the distortion due to the filter operator) and error due to the numerical method may cause steeper slope.

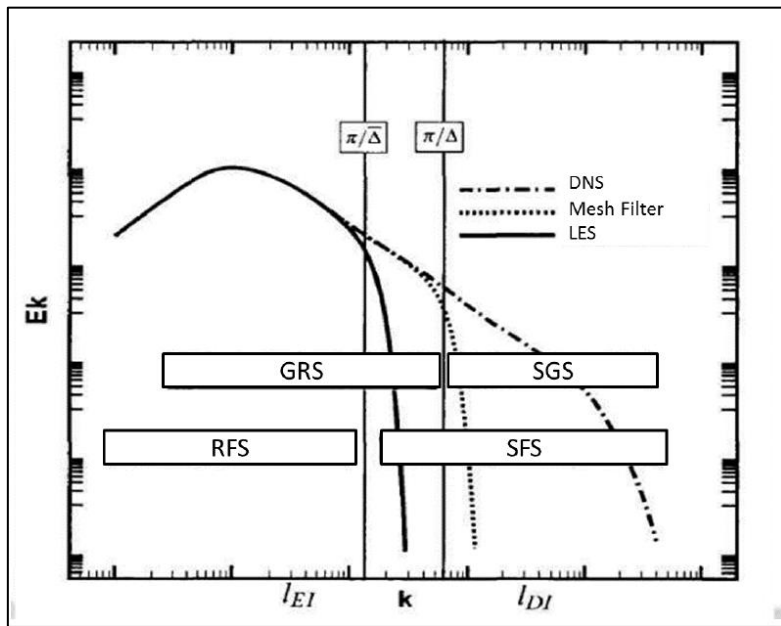


Figure 6 The difference in LES and DNS in the energy spectrum in terms of Kolomogorov's  $-5/3$  law

The image in Figure 7 The vertical structure is visualized by means of iso-surface of  $Q=3000$ . The surfaces areshows distinct asymmetries in the near-wake but yet with coherent vortical structures which partially also extend into the intermediate wake where the flow exhibits turbulent-like disorderly vortices. Also, the x-velocity histories at two points in Figure show the disorder of signal, a character of turbulence. Therefore, it is necessary to examine whether the flow at  $ReD = 10000$  has developed to turbulence. This part focuses on analysis of the flow state by means of Kolmogorov's  $-5/3$  law.

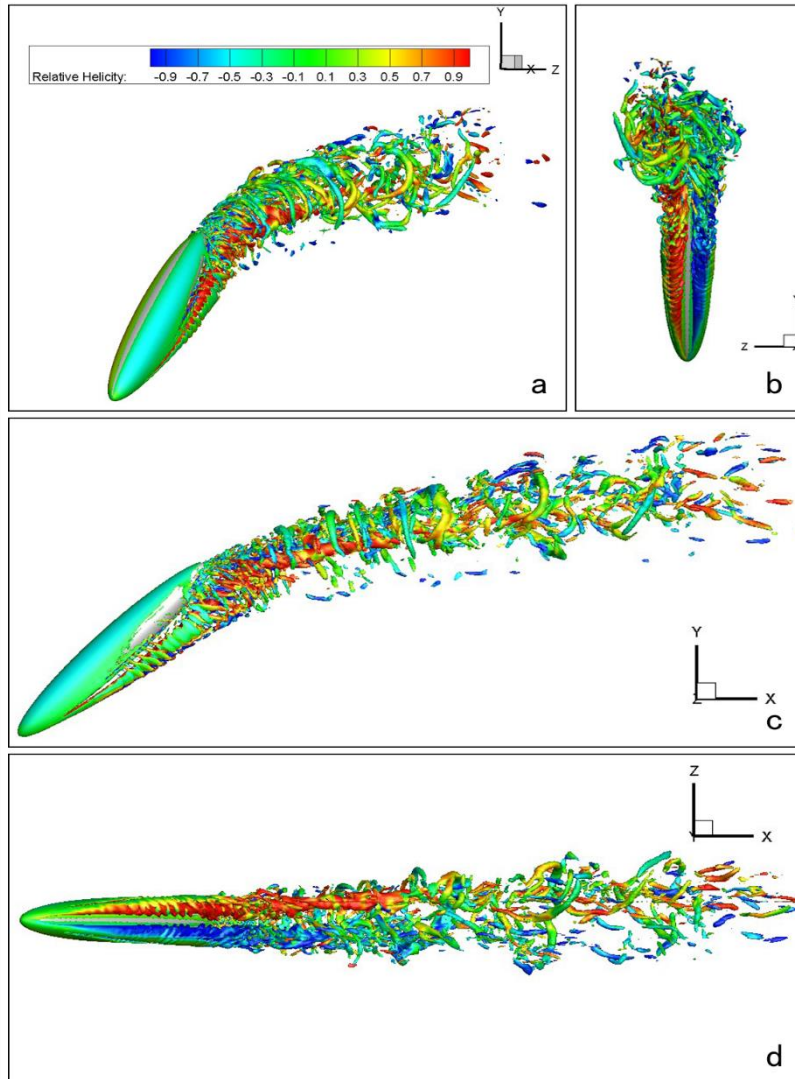


Figure 7 The vertical structure is visualized by means of iso-surface of  $Q=3000$ . The surfaces are flood by relative helicity. (a)perspective view (b)back view (c)side view (d)upward view

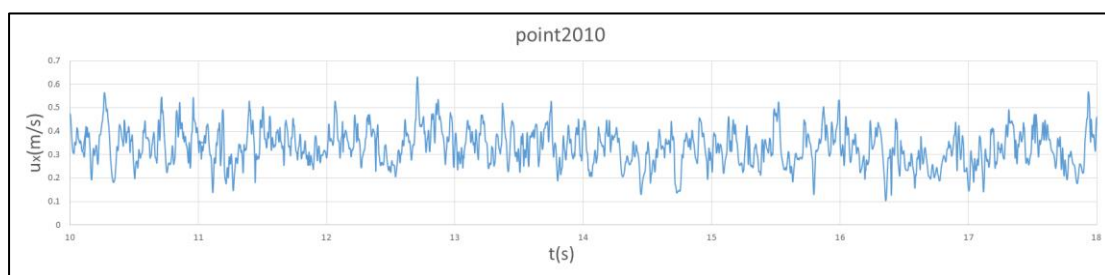
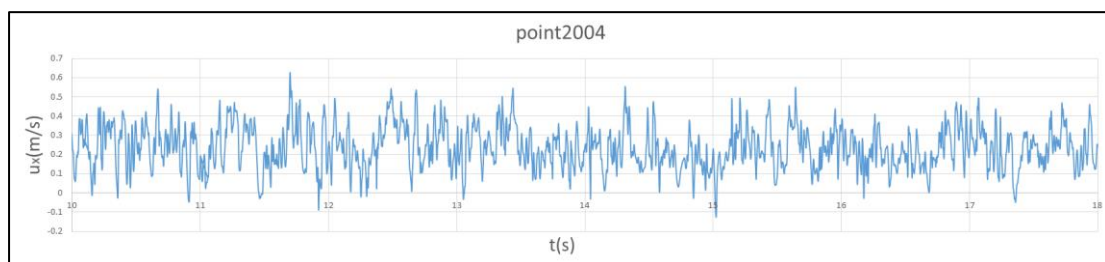


Figure 8 The x-velocity signal at two monitor points

### 4.3 The discussion on energy dissipation and numerical error in LES

#### 4.3.1 The impact of filter operation

In this part, the effect of filter operator on energy spectrum will be discussed first. As mentioned in Section 2, in LES only the contribution of the large, energy-carrying structures to momentum and energy transfer is computed exactly, and the effect of the small scales of turbulence is modelled, which is achieved through the filter operation, the most important turning point for LES. While the large eddies part still gets solved, the small eddies part is considered as isotropic, where the SFS was introduced. This is why the filter operator itself will have an impact on the solution. Let us take three operation as an example in Table to understand their effect on energy spectrum.

Table 3 Three filter operations

	Physics Space	Spectral Space
Spectral	$\frac{\sin(\pi x/\bar{\Delta})}{\pi x}$	$\begin{cases} 1, &  k  \leq \pi/\bar{\Delta} \\ 0, &  k  > \pi/\bar{\Delta} \end{cases}$
Box	$\begin{cases} 1/\bar{\Delta}, &  x  \leq \bar{\Delta}/2 \\ 0, &  x  > \bar{\Delta}/2 \end{cases}$	$\frac{\sin(k\bar{\Delta}/2)}{(k\bar{\Delta}/2)}$
Gaussian	$\left(\frac{\gamma}{\pi\bar{\Delta}^2}\right)^{1/2} \exp\left(-\frac{\gamma x^2}{\bar{\Delta}^2}\right)$	$\exp\left(-\frac{k^2\bar{\Delta}^2}{4\gamma}\right)$

As can be seen from the formulae of operators, both the Box and Gaussian method have high frequency component in the modelling process, in contrast to the Spectral method that only performs this treatment on the low frequency region while on the high frequency region maintains the “DNS shape”. Therefore, the impact of the Box and Gaussian method will be exerted on the whole frequency region, which will result in the distortion of the spectrum from LES in comparison with that from DNS. The filter method used in Fluent is kind of different with these three operators. In the process of spatial discretization, the finite volume method itself has provide the filter operator among the control volume. As we can apply such operator to the whole physical space, the method used in Fluent, called Implicit Filter, also causes some distortion in the whole frequency range. In addition, the dissipation region on the energy spectrum will definitely get distorted to some degree, with small eddies being modeled. However, such effect is not confined in dissipation region; the region out of the filter scale will all be impacted as well.

The impact of filter is not confined in frequency region; it also causes problems in the measurement of force. To facilitate the discussion, SFS term is defined as  $\partial\tau_{ij}/\partial x_j$  and total nonlinear term  $\partial\bar{u}_i\bar{u}_j/\partial x_j$ . In ideal LES, the sum of these two terms is equal to the full nonlinear term  $\partial\bar{u}_i\bar{u}_j/\partial x_j$ . However, in practice, the contribution to the total nonlinear depends on the SFS model used. One thing deserved to be mentioned is the importance of accurately representing the SFS term in the cases where the SFS term accounts for a larger proportion of the total force. However, numerical error also becomes more significant because fine-scale motions are not well-represented on the grid [25]. That is how the SGS model have an influence on the force. However, even if the SFS model is perfect, the filter size chosen also plays an important role, see Figure . The result of two dominant frequency

St1=0.1462 and St2=0.2436 obtained from the Fourier transform of the force  $F = \sqrt{F_x^2 + F_y^2 + F_z^2}$ . Unlike DNS, where  $St2 \approx 2St1$ , the double relationship in present study is not perfect, with  $St2 \approx 1.7St1$ , which might be resulted from the SGS model and filter size; while to what extent that these factors influence the results is still unknown.

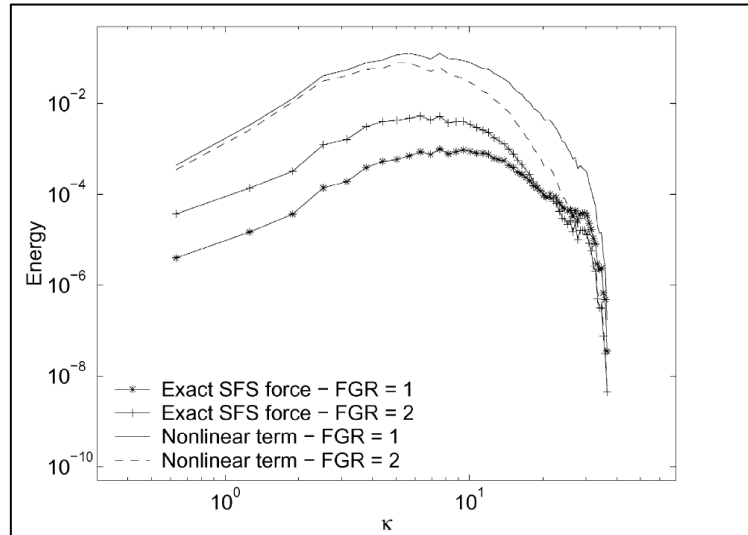


Figure 9 Energy spectra of the spectrally computed nonlinear term and the SFS term for a fixed resolution (323 grid) and filter-grid ratios of one and two.<sup>[25]</sup>

#### 4.3.2 The numerical error in LES

LES of turbulent flows are normally performed on grids that satisfy the need to resolve the important large flow structures, and numerical errors on such grids can have considerable effects on simulation results. In Navier-Stokes equations, numerical errors have different effects on different forms of nonlinear terms, which depends on the numerical schemes used.

Numerical errors are usually divided into two types: truncation error (or discretization error) and aliasing error. Truncation errors, one of two sources of error in finite difference methods, result from discrete approximation of derivatives in simulations, which can exceed the magnitude of the SFS term for low-order finite-difference simulations. One thing should be mentioned is that finite-difference schemes show large errors at high wavenumbers. Even if more accurate finite-difference methods can provide better approximations at higher wavenumbers, the accuracy is always better at low wave-numbers than at high wavenumbers, see Figure . Another type of error, Aliasing error, occurs whenever nonlinear terms are multiplied in physical space and calculated numerically, which can have an influence on SFS term and thereby the results of simulation mentioned in 0; high frequency components produce higher ones which cannot be adequately represented on a finite grid. Thus, the frequencies beyond the grid wavenumber cutoff are incorrectly “aliased” to wavenumbers that are resolved. This type of error can be removed, but this is computationally expensive, even in spectral codes where the 3/2-rule for dealiasing is applicable and is relatively straightforward to implement, and complete dealiasing is difficult in complex geometries <sup>[25]</sup> [26].

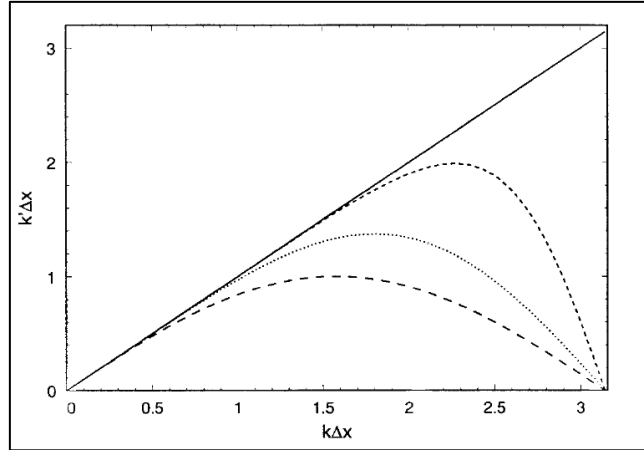


Figure 10 Modified wavenumbers: (—) Spectral; (—) 2nd order finite difference; (··) 4th order finite difference; (- - -) 6th order Pade' one also needs to employ the identity scheme.

A. G. Kravchenko and P. Moin have studied the effect of truncation and aliasing errors [26]. They performed numerical simulations of turbulent channel flows using spectral and various finite difference methods. From their study, the conclusion was drawn that in low-order finite-difference schemes, the high wavenumber part of the energy spectrum is heavily distorted by truncation errors. One way to avoid this distortion is to increase the order of the finite-difference method, which can both improve the results of LES and the performance of a subgrid-scale model. As shown in Figure, the results of LES become closer to that obtained by spectral method with the order of finite-difference scheme increasing. When the 2nd order finite difference method is applied, the energy spectra exhibit steeper slope than that obtained by 6th order finite difference and spectral method in the high wavenumber part, i.e. high frequency region, where the slopes in Figure steeper than Kolomogorov's reference line. In present study, the least square cell based method is used, a 2nd order method for pressure and bounded central differencing method for momentum. Therefore, it is reasonable to assume that this 2nd order finite difference might result in the steeper slope and the flow field at  $ReD = 10000$  has developed to turbulent state. While this assumption need to be further examined by more accurate finite difference schemes.

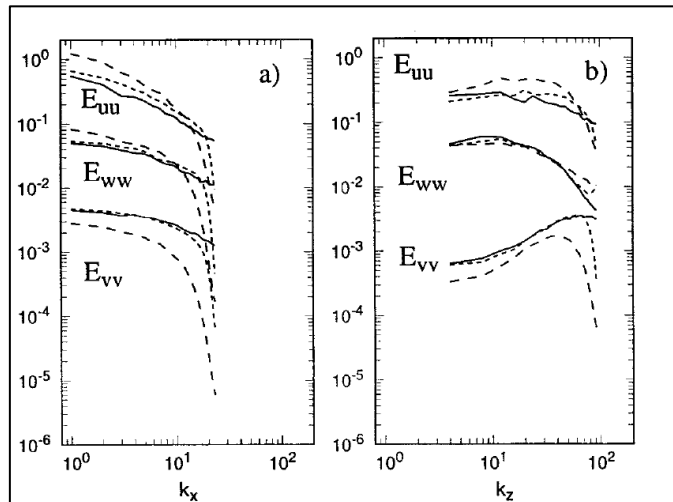


Figure 11 One-dimensional energy spectra at  $y^+=15$  in LES: (—) spectral; (- - -) 2<sup>nd</sup> order finite difference; (- · -) 6<sup>th</sup> order Pade' scheme; (a) streamwise; (b) spanwise. [26]

## 5 Conclusion

In this paper, the wake instability and flow state were analyzed. The relevant instability of the asymmetric wake behind the prolate spheroid was attributed to global instability, as we rule out initial perturbation that was required for the convective instability. Then the detailed analysis on the frequency was conducted by means of simple FFT. Two dominant frequencies were observed at  $St_1=0.1462$  and  $St_2=0.2436$  from the Fourier transform of  $F$ , while  $St_1$  and  $St_2$  were hard to be distinguished from energy spectra because of the error caused by simple FFT and the shortage of data.

As the flow at  $ReD = 10000$  exhibited some turbulence-like features and the view of flow structures and x-velocity signals were not able to provide sufficient information, we analyzed the flow state by Kolmogorov's  $-5/3$  law and the results seemed that the flow did not develop to turbulent flow.

However, it is not reasonable to determine the flow state when the steeper slope was observed, taking the energy dissipation and numerical error of LES into consideration. We found that filter operation and truncation and aliasing errors would have effects for the energy spectrum, and more accurate methods were necessary to authenticate our assumption.

## References

- [1] El Khoury G.K., Andersson H.I., and Pettersen B. Crossflow past a prolate spheroid at Reynolds number of 10 000. *Journal of Fluid Mechanics*, 2010, 659: 365-374
- [2] N Wikström , U Svennberg , N Alin & C Fureby (2004) Large eddy simulation of the flow around an inclined prolate spheroid, *Journal of Turbulence*, 5, N29
- [3] A, Karlsson and C. Fureby, LES of the Flow Past a 6:1 Prolate Spheroid, 47th AIAA Aerospace Sciences Meeting Including The New Horizons Forum and Aerospace Exposition, 5–8 January 2009, Orlando, Florida
- [4] Jiang F, Gallardo J P, Andersson H I, et al. The transitional wake behind an inclined prolate spheroid [J]. *Physics of Fluids*, 2015, 27(9):093602.
- [5] Jiang F, Gallardo J P, Andersson H I. The laminar wake behind a 6:1 prolate spheroid at 45° incidence angle [J]. *Physics of Fluids*, 2014, 26(11):113602.
- [6] Pierre Sagaut, Introduction to large scale eddy simulation for incompressible fluids flows, *Aerospace Science and Technology*, 1998, no.6, 413–414
- [7] Leonard A. 1975 Energy cascade in large eddy simulations of turbulent fluid flows. *Adv. Geophys.* 18A, 237–248.
- [8] G. Q. Chen, L. Tao and K. R. Rajagopal, Remarks on large eddy simulation, *Communications in Nonlinear Science & Numerical Simulation*, September 2000
- [9] H.-J. Kim, S. Lee, and N. Fujisawa, Computation of unsteady flow and aerodynamic noise of NACA0018 airfoil using large-eddy simulation, *International Journal of Heat and Fluid Flow* 27 (2006) 229–242
- [10] François Beaubert and Stéphane Viazzo, Large Eddy Simulation of a plane impinging

- jet, C. R. *Mecanique* 330 (2002) 803–810
- [11]C. Fureby, Towards the Use of Large Eddy Simulation in Engineering, 46th AIAA Aerospace Sciences Meeting and Exhibit, 7–10 January 2008, Reno, Nevada
- [12]Gordon Erlebacher and Mohammed Y. Hussaini, Direct Numerical Simulation and Large Eddy Simulation of Compressible Turbulence
- [13]A. Feymark, M. Chapuis, C. Fureby and M. Liefvendahl, Large Eddy Simulation of High Re Number Partially Separated Flow, 50th AIAA Aerospace Sciences Meeting including the New Horizons Forum and Aerospace Exposition, 09–12 January 2012, Nashville, Tennessee
- [14]D.G.E. Grigoriadis, J.G. Bartzis and A. Goulas, Efficient treatment of complex geometries for large eddy simulations of turbulent flows, *Computers & Fluids* 33 (2004) 201–222
- [15]Parviz Moin, Advances in large eddy simulation methodology for complex flows, *International Journal of Heat and Fluid Flow* 23 (2002) 710–720
- [16]Trong T. Bui, A parallel, finite-volume algorithm for large-eddy simulation of turbulent flows, *Computers & Fluids* 29 (2000) 877–915
- [17]Roland Bouffanais, Advances and challenges of applied large-eddy simulation, *Computers & Fluids* 39 (2010) 735–738
- [18]A. Sohankar, Flow over a bluff body from moderate to high Reynolds numbers using large eddy simulation, *Computers & Fluids* 35 (2006) 1154–1168
- [19]CFD Online, [https://www.cfd-online.com/Wiki/Smagorinsky-Lilly\\_model](https://www.cfd-online.com/Wiki/Smagorinsky-Lilly_model)
- [20]AIAA, The Asymmetric Vortex Wake Problem - Asking the Right Question, AIAA Fluid Dynamics Conference & Exhibit , 2006 , 8 (9) :404-413
- [21]A. Ayoub and K. Karamcheti, An experiment on the flow past a finite circular cylinder at high subcritical and supercritical Reynolds numbers, *J. Fluid Mech.* 118, 1 - 26 (1982).
- [22]B. Ma and T. Liu, Low-frequency vortex oscillation around slender bodies at high angles of attack, *Phys. Fluids* 26, 091701(2014).
- [23]Tikhomirov V.M. (1991), Equations of Turbulent Motion in an Incompressible Fluid. In: Tikhomirov V.M. (eds) Selected Works of A. N. Kolmogorov. Mathematics and Its Applications (Soviet Series), vol 25. Springer, Dordrecht
- [24]Stephen B.Pope. Turbulent flows, Cambridge University Press,2000, 99-044583
- [25]Fotini Katopodes Chow and Parviz Moin, A further study of numerical errors in large-eddy simulations, *Journal of Computational Physics* 184 (2003) 366–380
- [26]A. G. Kravchenko and P. Moin, On the Effect of Numerical Errors in Large Eddy Simulations of Turbulent Flows, *Journal of Computational Physics* 131, 310–322 (1997)